Title: Preparation, characterization and photocatalytic activity of lanthanum and vanadium co-doped mesoporous TiO_2 for azo-dye degradation

Author: Jelena Nešić Dragan D. Manojlović Ivan Anđelković Biljana P. Dojčinović Predrag J. Vulić Jugoslav Krstić Goran M. Roglić

PII: S1381-1169(13)00224-0
DOI: http://dx.doi.org/doi:10.1016/j.molcata.2013.05.018
Reference: MOLCAA 8771

To appear in: *Journal of Molecular Catalysis A: Chemical*

Received date: 19-2-2013
Revised date: 13-5-2013
Accepted date: 14-5-2013

Please cite this article as: J. Nešić, D.D. Manojlović, I. Anđelković, B.P. Dojčinović, P.J. Vulić, J. Krstić, G.M. Roglić, Preparation, characterization and photocatalytic activity of lanthanum and vanadium co-doped mesoporous TiO_2 for azo-dye degradation, *Journal of Molecular Catalysis A: Chemical* (2013), http://dx.doi.org/10.1016/j.molcata.2013.05.018

Preparation, characterization and photocatalytic activity of lanthanum and vanadium co-doped mesoporous TiO_2 for azo-dye degradation

Jelena Nešić*[a], Dragan D. Manojlović[b], Ivan Anđelković[a], Biljana P. Dojčinović[c], Predrag J. Vulić[d], Jugoslav Krstić[e], Goran M. Roglić[b]

[a] *Innovation Center of the Faculty of Chemistry, University of Belgrade, Studentski trg 12, Belgrade, Serbia*

[b] *Faculty of Chemistry, University of Belgrade, Studentski trg 12, Belgrade, Serbia*

[c] *Institute of Chemistry, Technology and Metallurgy, Center of Chemistry, University of Belgrade, Njegoseva 12, 11000 Belgrade, Serbia*

[d] *Faculty of Mining and Geology, Department of Mineralogy, Crystallography, Petrology and Geochemistry, University of Belgrade, Djusina 7, 11000 Belgrade, Serbia*

[e] *Institute of Chemistry, Technology & Metallurgy, Department of Catalysis & Chemical Engineering, University of Belgrade, Njegoseva 12, 11000 Belgrade, Serbia*

* Corresponding author. Tel.: +381 65 4055911; fax: +381 11 2184 330

E-mail address: jelenanesic@chem.bg.ac.rs (Jelena Nešić)

Highlights

TiO_2 catalysts co-doped with La and V were synthesized using microwave-assisted hydrothermal process.

Changes in the morphology and photocatalytic activity were observed as amount of both dopants were altered.

The catalyst with 2% w/w La and 0.02% w/w V appeared to be the most photoactive.

V-La co-doped TiO_2 was easily separable by settling down and showed good stability and reusability.

Abstract

Titanium dioxide photocatalysts co-doped with lanthanum and vanadium were prepared by a facile microwave-assisted hydrothermal method and characterized by XRD, SEM, N_2 physisorption at 77 K and DRS. The characterization showed that co-doped TiO_2 samples have a high degree of crystallinity and existence of fully anatase phase. It was found that all the synthesized catalysts have the mesoporous structure. The co-doped TiO_2 samples have larger BET surface areas and the mesopores volume than pure TiO_2 and La doped samples. The vanadium co-doping contributes to the extension of absorption into the visible region. The photocatalytic activity of the samples was evaluated by the decolorization of textile dye Reactive Blue 52 in aqueous solutions under sun-like radiation. Compared with La singly doped TiO_2, the co-doped catalysts showed an important improvement of photoactivity. The photocatalyst with 2% w/w La and 0.02% w/w V appeared to be the most photoactive. Optimal catalyst loading and the kinetics of degradation were also studied. Demonstrating higher photodegradation efficiency for RB than commercially available TiO_2 Evonik P25, easy separation from suspension by spontaneous sedimentation and reusability of the catalyst, make this photocatalyst suitable for wastewater treatment.

Keywords: Microwave; Mesoporous titanium dioxide; co-doped; Lanthanum; Vanadium; Reactive Blue 52.

1. Introduction

Toxic wastes have been continuously released into the air and water, leading to serious environmental and health problems. Conventional methods of water treatment as coagulation, carbon adsorption, reverse osmosis, ultrafiltration and similar, as well as biological treatment, could not remove some organic pollutants efficiently. Advanced oxidation processes, developed in recent decades, are probably the best alternative for removal of hardly biodegradable pollutants [1,2] and also for removing pathogens [3]. These degradation techniques are based on the generation of reactive oxygen species like hydroxyl (OH•) and hydroperoxyl (HO_2•) radicals.

Among the advanced oxidation processes, photocatalysis with titanium oxide-based catalysts is very promising in the field of environment remediation. Photo-assisted processes are clean, safe and efficient. Most of commonly used semiconductors in photocatalytic processes are stable and nontoxic, thus, they are environmentally acceptable. These systems are open-atmospheric, which can operate at room temperature, utilizing natural solar light as energy source, so they are cost-effective [4].

Nevertheless, these processes suffer from limitations. TiO_2 catalysts can only absorb the UV portion of the solar spectrum (wavelength < 388 nm), which comprises just 4-6% of the solar radiation. This problem is partially overcome by doping with different species which allows reactions could be induced not only with UV, but also visible light. The most common dopants used for this purpose are transition metals like iron [5,6], copper [7], tungsten [8], vanadium [9,10], cobalt [11], molybdenum [12], manganese [13], chromium [14].

Transition metals ion doping can narrow the energy gap through the formation of new impurity energy levels in TiO_2. Introduction of such energy levels in the band gap induces the red shift in the band gap transition and the visible light absorption. Metal ion dopants act as electron (or hole) traps and alter e^-/h^+ recombination rate, according to the following mechanism:

$M^{n+} + e_{cb}^{-} \rightarrow M^{(n-1)+}$ (electron trap)

$M^{n+} + h_{vb}^{+} \rightarrow M^{(n+1)+}$ (hole trap)

where the energy level for $M^{n+}/M^{(n-l)+}$ lies below the conduction band edge (E_{cb}) and the energy level for $M^{n+}/M^{(n+l)+}$ above the valence band edge (E_{vb}) [15]. Doping does not only allow visible light absorption, but the presence of trap sites within the TiO_2 bands may increase the lifetime of photoinduced charge carriers. Metal ions also may act as recombination sites for photoinduced charge carriers, so they can reduce the quantum efficiency. Influence on the recombination rate and hence, increase or decrease in the photocatalytic activity, depends on the nature and amount of doping agent. Thus, the possible limitations in the use of transition metal doped TiO_2 are promoted charge recombination at metal sites and thermal instability.

Doping with lanthanide ions was proven to increase thermal stability, arrest agglomeration and stabilize the mesoporous structure [16]. Lanthanide ions have the ability to form complexes with various Lewis bases (e.g., alcohols, amines, thiols), due to the interaction of their *f*-orbitals with different functional groups. Providing high surface area and forming complexes, incorporation of lanthanide ions concentrate the organic pollutants on the semiconductor surface. Lanthanides doping improves the photocatalytic activity by increasing the adsorption capacity for organic compounds, as well as, suppress electron-hole recombination rates during the process of photocatalytic reaction [17].

Since the doping with transition metals and lanthanide ions has its respective advantage, it can be assumed that doping with two dopants can show synergetic effect in improving photocatalytic activity. It has been reported [18] that co-doping with Fe and La shows significant improvement on the photocatalytic activity compared with single element doping into TiO_2. The goal of this work was to prepare La doped and V,La co-doped TiO_2 materials and investigate the potential synergetic effect of these two dopants for degradation of textile dyes. In this paper, TiO_2 photocatalysts were prepared by microwave-hydrothermal method. This method was chosen because the conventional hydrothermal process is often very time and energy consuming [19,20]. Microwave-hydrothermal technique compared to conventional hydrothermal process, allows rapid heating to the required temperature and extremely rapid rates of crystallization [21,22]. Prepared materials are characterized with X-ray diffraction (XRD), scanning electron microscopy (SEM), N_2 physisorption at 77 K, UV–vis diffuse reflectance spectroscopy (DRS) and the content of La, V and Ti in the synthesized samples was determined by inductively coupled plasma–optical emission spectroscopy (ICP–OES) technique. For the best one, catalyst loading and the kinetics of degradation were also studied and its photodegradation rate compared to commercially available Evonik P25 powder.

2. Materials and methods

2.1. Materials

Titanium tetrachloride, $TiCl_4$ (Fluka 98%), was used as the starting material. Lanthanum (III) nitrate hexahydrate, $La(NO_3)_3 \cdot 6H_2O$ (Merck), ammonium metavanadate, NH_4VO_3 (Merck), ammonium hydroxide, NH_4OH (Sigma-Aldrich 25%) were used as received. Commercial reactive

azo dye used in the experiments was Reactive Blue 52 (RB) (Clariant, Switzerland), the molecular structure is shown in Fig. 1. The water used throughout was deionized, with conductivity between 1.0 and 1.5 μS/cm.

Fig. 1. Molecular structure of Reactive Blue 52.

2.2. Synthesis of pure and metal doped mesoporous TiO_2

All catalysts were prepared using the microwave-hydrothermal method. $TiCl_4$ was dropped on ice made from distilled water ($TiCl_4$:H_2O (v/v) ratio 1:10) and homogeneous and transparent solution was obtained. Then, the solution was subjected to precipitation by the slow addition of $NH_4(OH)$ (30%) solution under constant stirring at room temperature. The hydrolysis was controlled with the addition of $NH_4(OH)$, until the reaction mixture attains a pH between 7 and 8. Precipitate was obtained and the suspension was transferred into a Teflon microwave closed vessels (digestion system ETHOS 1 Milestone, equipped with a High Pressure Rotor SK-10, Italy), sealed and heated by microwave irradiation reaching a maximum temperature of 150 °C in 10 min, then kept at this temperature for 15 min more for hydrothermal treatment. The resulting product was separated by centrifugation and washed repeatedly with deionized water until the precipitate becomes free of chloride ion (confirmed by $AgNO_3$ test). Finally, it was dried at 80 °C for 5 h and then calcined at 500 °C for 10 h.

Doped TiO_2 samples were prepared according to the above procedure including metal salts in water to give an appropriate level of dopants. The samples with the La nominal contents of 0.2, 2 and 4%, w/w (labeled as 0.2La/TiO_2, 2La/TiO_2 and 4La/TiO_2) and the samples with La 2%, w/w and V nominal contents of 0.01, 0.02 and 0.05%, w/w (labeled as 0.01V-2La/TiO_2, 0.02V-2La/TiO_2 and 0.05V-2La/TiO2) were prepared. All the dopant concentrations mentioned in this work are the weight percent.

2.3. Characterization

The content of La, V and Ti in the synthesized samples was determined by inductively coupled plasma–optical emission spectroscopy (ICP–OES) technique (Thermo Scientific iCAP 6500 Duo ICP spectrometer, United Kingdom). Before measurements, about 0.1g of each sample was decomposed in a microwave closed vessel digestion system with acid mixture of 5 ml of sulphuric acid (H_2SO_4, 98%), 2 ml of nitric acid (HNO_3, 65%) and 1 ml of hydrofluoric acid (HF, 50%), all analytical grade reagents from Carlo Erba. The maximum temperature of 220 °C reached during 15 minutes and then this temperature kept constant for 20 minutes more.

Scanning electron micrographs were recorded on an automated scanning electron microscope (SEM), JSM-6610LV JEOL.

Powder X-ray diffraction (XRPD) was used for identification of crystalline phases, quantitative phase analysis and estimation of crystallite size and strain. The XRPD patterns were collected with Philips diffractometer (PW1710) employing CuKα1,2 radiation. Step scanning was performed with

2θ ranging from 20 to 100°, step size of 0.080° and the fixed counting time of 5 s per step. The XRPD patterns were used to refine crystallographic structure and microstructural parameters using the procedure implemented in the FullProf computer program [23].

Adsorption–desorption isotherms were obtained by nitrogen adsorption at 77 K using a Sorptomatic 1990 Thermo Finnigan device. Prior to adsorption, the samples were degassed for 1 h at room temperature under vacuum and additionally 16 h at 110 °C at the same residual pressure. The specific surface area of samples (S_{BET}) was calculated by applying the Brunauer–Emmet–Teller equation, from the linear part of the adsorption isotherm [24]. The total pore volumes (V_{tot}) were obtained from the N_2 adsorption, expressed in liquid form, by applying Gurevitsch's rule [25]. Micropore volumes (V_{mic}) were estimated according to the Dubinin–Radushkevich method [26]. Mesopore volumes (V_{mes}) were estimated according to the Barrett, Joyner and Halenda method from the desorption branch of the isotherm [27].

Diffuse reflectance spectroscopy was carried out using a Perkin-Elmer Lambda 900 UV-vis-NIR spectrometer provided for with a PELA-1000 accessory within the wavelength range of 200-800 nm and a resolution of 1 nm. The absorption of the samples was plotted in Kubelka-Munk (KM) arbitrary units vs. wavelength. The reflectance of MgO was used as reference.

2.4. Photodegradation procedure and sorption

A cylindrical photochemical reactor, with a water circulation arrangement to maintain the temperature in the range 22 ± 1 °C was used in all experiments. The light was provided by an Osram Ultra-Vitalux lamp (300W) with sun-like radiation spectrum. The distance between the source of light and the sample was 25 cm. Appropriate amount of photocatalysts were added into 100 mL of RB solution (native pH) and stirred in the dark for 4 h before illumination, to ensure the establishment of an adsorption–desorption equilibrium between the photocatalyst and RB. After adsorption–desorption equilibrium was reached, the adsorbed amount of RB was estimated from the change in dye concentration. Concentration changes of the RB were monitored according to the decreasing intensity of the absorption peak at 615 nm. During irradiation, stirring was maintained to keep the suspension homogeneous and 4 ml aliquots of the aqueous suspensions were collected at regular intervals, then centrifuged and spectra of the supernatant were measured with an UV-VIS spectrophotometer (Cintra 10 UV-Visible Spectrometer, Australia). Sedimentation rate of catalyst was determined by measuring the turbidity in Formazin Turbidity Units (FTU) using a turbidimeter (HANNA Instruments, LP-2000, Italy). Turbidimetric measurements were performed at constant temperature of 22 ± 1 °C.

3. Results and discussion

3.1. Structural characteristics

3.1.1. X-ray diffraction analysis of photocatalysts

XRPD analyses patterns shows that the most intensive diffraction peaks in the XRD patterns of produced samples can be ascribed to the anatase crystal structure (JCPDS card 78-2486). The

presence of broad low-intensity diffraction peak at $2\theta \approx 30.8°$, which can be ascribed to the brookite phase of TiO_2, is observed in pure TiO_2 sample XRD pattern (JCPDS card 29-1360). Brookite content in this sample can be estimated less than 3%. Structure refinements were performed by the Rietveld method. The final Rietveld refinement plots of the samples are presented in Fig. 2., while the main results of the refinement are listed in Table 1. The obtained values for the unit cell parameters of anatase show that the value of the parameter *a* varies around its reference value (a_0 = 3.78479(3) Å), while the value of the *c* parameter in all the samples is slightly smaller than the reference one (c_0 = 9.51237(12) Å).

Fig. 2. The final Rietveld refinement plots of the samples: a) TiO_2; b) $2La/TiO_2$; c) $4La/TiO_2$; d) $0.01V\text{-}2La/TiO_2$; e) $0.02V\text{-}2La/TiO_2$; f) $0.05V\text{-}2La/TiO_2$. Observed data are represented by circles and calculated data by continuous line. Bragg positions are denoted by vertical ticks, and difference curve is shown in the bottom.

Low values of agreement factors between the model, both structure and microstructure, and XRD data (Table 1) indicates high accuracy of the obtained results.

The ionic radius is the most important condition, which can strongly influence the ability of the dopant to enter into TiO_2 crystal lattice. The ionic radius of La^{3+} (0.115 nm) is bigger than that of Ti^{4+} (0.068 nm). Therefore, it is difficult for La^{3+} to really enter the lattice of TiO_2 powder. La^{3+} ions are most likely to be found as dispersed metal oxides within the crystal matrix or on the surface of TiO_2. It can be seen that no obvious diffraction peaks that could be attributed to the dopants were observed. Probably, La^{3+} ions were dispersed uniformly onto TiO_2 nanoparticles as the form of small clusters La_2O_3, in the range undetectable by XRD. But, since the ionic radii of V^{4+} (0.058 nm) and V^{3+} (0.064 nm) ions are close to that of Ti^{4+}, it is expected that V^{3+}/V^{4+} ions will incorporate in the TiO_2 lattice. No diffraction peaks corresponding to vanadium oxide were observed. Therefore, the V ions were either highly dispersed in the TiO_2 matrix or formed small oxide clusters having sizes and/or concentrations beyond the detection limit of diffractometer.

The obtained average crystallite size slightly decreases with increase of the content of La in the first group of the samples, and V in the second sample group. This reduction in crystallite size is probably due to segregation of the dopant cations at the grain boundary, which inhibits the grain growth by restricting direct contact of grains [16].

Table 1. The results of the Rietveld analyses of anatase phase (unit cell parameters, microstructure parameters and refinement residuals).

3.1.2. SEM imaging of photocatalysts

The SEM analysis was carried out in order to determine the morphology of the La doped and V-La co-doped TiO_2 samples. SEM micrographs are shown in Fig. 3. It is observed that synthesized samples consist of mainly spherical aggregates. These aggregates are polydisperse in size with diameters ranging from several tens to several hundreds of nanometers. The SEM images show that the addition of both dopants changes the morphology of particles - increasing the amount of dopants, size of spherical aggregates are reduced.

Fig. 3. SEM images: (a) TiO_2. (b) 0.2La/TiO_2. (c) 2La/TiO_2. (d) 4La/TiO_2. (e) 0.02V-2La/TiO_2. (f) 0.05V-2La/TiO_2, line bar 0.5 μm.

3.1.3. Nitrogen physisorption

Information about specific surface area, pore volume and pore diameter of catalysts were summarized in Table 2. The pure TiO_2, synthesized by microwave method, has a relatively large surface area (for example, specific surface area of commercially available TiO_2 Evonik P25 is 51.0 m^2 g^{-1}) and this characteristic of material can be attributed to the method of synthesis. Also, the specific surface area of the samples is dependent on the La and V content. It can be seen that the specific surface area increases progressively with increasing La content up to 2%, then the sample with 4% of La has only slightly larger surface area compared to the sample with 2% of La. Similar trend is observed for the samples co-doped with different amounts of V.

The isotherms of all synthesized materials presented in Fig. 4 and 5 can be interpreted [24] as type IV with an H2 type hysteresis loop, which is typical for mesoporous materials. All the isotherms show big stepwise between adsorption and desorption and retain the shape of the loop compared to undoped TiO_2 sample. The increase of the La and V content affects pore diametar and volume, as follows, the mesopores volume increases and the diameter decreases with increasing concentration of both dopants. As shown in the insets of Fig. 4 and 5, the narrow pore size distribution curves for all materials are obtained.

The origin of increase in the specific surface area could be caused by a decrease in particle size and/or due to the formation of new phase, which has a higher specific surface area. SEM micrographs have confirmed the reduction of particle size with increasing the amount of dopants. However, this cannot be the only explanation for the increase in specific surface area, since the particle size reduction would also lead to preservation or reduction of the specific pore volume. Hence, it is obvious that the addition of dopants changes the textural properties also through the formation of a new phase.

Fig. 4. Nitrogen physisorption isotherms at 77 K of pure TiO_2 and La doped TiO_2. Empty symbols represent adsorption points and filled symbols represent desorption points

Fig.5. Nitrogen physisorption isotherms at 77 K of 2La/TiO_2 and V-La co-doped TiO_2. Empty symbols represent adsorption points and filled symbols represent desorption points

Table 2. Textural and structural properties of TiO_2 samples doped with different La and V content.

3.1.4. UV–vis diffuse reflectance spectra

The UV–vis diffuse reflectance spectra of synthesized samples are shown in Fig. 6. It is visible from the spectra that the curve shape of the spectrum of TiO_2 nanoparticles almost do not change after La^{3+} was doped, only slightly red shift of absorption edge is exhibited, attributed to the charge-transfer transition between La^{3+} ion *f* electrons and the TiO_2 conduction or valence band [28]. For co-doped samples, one additional peak can be noticed in visible region. Pure V_2O_5 shows two major

peaks at ~476 and 338 nm [29]. Therefore, this additional peak, which increases with increasing the amounts of vanadium, can be attributed to the presence of crystalline V_2O_5 species on the surface of the TiO_2. When vanadium is bulk-doped in TiO_2, instead of this peak, spectra exhibited the new long-tailed absorption in the visible light region up to ~779 nm [29,30].

Fig.6. Diffuse reflectance spectra of of pure, La-doped and V-La co-doped TiO_2 powders.

3.2. Photocatalytic degradation of RB textile dye

3.2.1. Determination of the optimal amount of dopants for the best performance of photocatalysts

Photocatalytic performance of the samples was evaluated by investigating the kinetics of the degradation of RB dye in aqueous suspensions. Fig. 7 shows the kinetics of the disappearance of RB from an initial concentration of 100 mg L^{-1} in the presence of La doped and V-La co-doped catalysts. The data presented in Fig. 7 a) show that catalysts doped with La show higher catalytic activity than pure TiO_2. The optimal amount of lanthanum doping is 2%. Further increase of the lanthanum content leads to the decrease of photoactivity, although the photoreactivity of 4% La doped TiO_2 is still higher than undoped TiO_2.

Therefore, the catalyst with 2% of the lanthanum was chosen for co-doping with vanadium in order to examine whether it improves photoactivity or might have detrimental effect. From Fig. 7 b), it can be seen that the addition of vanadium to the sample with an optimal amount of lanthanum significantly improves the photoactivity. It can be noticed a similar trend as in Fig. 7 a), there is an optimal concentration of vanadium.

Fig.7. Photocatalytic disappearance of RB using a) La doped and b) V-La co-doped TiO_2. Operating conditions: $[RB]_0$ = 100 mg L^{-1}, photocatalysts = 1 g L^{-1} and native pH.

The mechanism of TiO_2-photocatalyzed reactions has been the subject of numerous studies [31]. It is widely recognized that conduction band electrons (e^-) and valence band holes (h^+) are generated when aqueous TiO_2 suspension is irradiated with light energy greater than its band gap energy. The photogenerated electrons could reduce the dye or react with O_2 adsorbed on the catalyst surface, reducing it to superoxide radical anion $O_2^{\bullet-}$. The photogenerated holes can oxidize the organic molecule or react with OH^- or H_2O, oxidizing them into OH• radicals, which are powerful oxidants in degrading organics. For effective degradation, the organic pollutants should be pre-concentrated at the semiconductor surface in order to effectively trap the respective reactive radicals. It can be seen from morphology and the textural properties in Table 2, that lanthanum doping increases specific surface area and pore volume and thus provides more adsorption sites.

Also, reduced e^-/h^+ recombination rate improves the photoactivity [32]. An effective method to achieve the separation of e^- and h^+ is to introduce defects into TiO_2 lattice [33]. XRD results show that the crystal phase of La_2O_3 was not detected, even for catalyst with 4% of La. It was already explained in XRD results. Due to the relatively large size difference between La^{3+} and Ti^{4+}, it is difficult for lanthanum to substitute titanium ions in TiO_2 lattice. La^{3+} ions were probably dispersed uniformly onto TiO_2 nanoparticles as the form of small cluster La_2O_3. But titanium ion might substitute lanthanum atom in the lattice of La_2O_3 alternatively, and a Ti–O–La bond could be formed [17]. In that way, an imbalanced charge would occur and shallow trapping sites for charge carriers (e^- or h^+) would form, thereby separating the arrival time of e^- and h^+ at the surface and increasing the photocatalytic efficiency. At high concentration, these trapped e^- or h^+ might recombine together before migrating to the surface, resulting in lower photocatalytic activity of TiO_2, because all the reactions take place only on the surface.

The V-La co-doped TiO_2 exhibits a higher photocatalytic activity for the degradation of RB than pure and La doped TiO_2. This may be owing to the synergistic effects of dopants. In literature, bulk doping V ions has detrimental effects, but doping V ions in the surface lattice significantly improves the photocatalytic activity [30]. Migration of ions in a solid matrix is controlled by the Tammann temperature; the-temperature high enough to make ions or atoms of the bulk of a solid, sufficient mobile for bulk-to-surface migration. V_2O_5 has a low melting point, and hence high mobility under mild temperature conditions. In this case, calcination temperature was sufficiently high (500 $^\circ$C) to drive the diffusion of V ions (Tammann temperature of 209 $^\circ$C). The migration mechanism of V_2O_5 on the surfaces is not yet understood in detail, but published results indicate that a process of defect diffusion through the vanadia monolayer is involved [34]. In XRD results, the crystal phase of V_2O_5 was not detected, probably due to low concentration of V ions. Segregation of crystalline V_2O_5 from the lattice on the surface of TiO_2 is proven by DRS.

Vanadium ions in the surface layers, resulted in the segregation of V_2O_5 clusters, promote anatase to rutile phase transformation and caused poor crystallinity [30]. In addition, high concentrations of V ions cause over accumulation of electrons in the TiO_2 and accelerate the charge recombination and reduced the photocatalytic activity. Thus, there is an optimal amount of V ions for the the most efficient photocatalytic process. As can be seen in Fig. 7 b), the most efficient catalyst is 0.02V-2La/TiO_2, indicating the optimal amount of both dopants necessary to obtain their synergistic effects and above which the recombination rate of electrons and holes becomes too fast [35].

In order to explain the enhanced activity of co-doped TiO_2, possible mechanism was proposed in Fig. 8. Appropriate amount of surface V_2O_5 is necessary. Since the ionic radii of V and Ti ions are very similar, it is expected that the part of V ions is incorporated in the TiO_2 lattice. And due to very low Tammann temperature of V_2O_5, the part of V ions is segregated in the surface layers, resulted in the segregation of V_2O_5 clusters. The presence of V^{5+} ions in the form of V_2O_5 (semiconductor with band gap of 2 eV) produces a space charge layer at the interface with TiO_2 due to difference in electrochemical potential [36]. The stationary electric field at the interface provides the driving force to the photogenerated e^- on TiO_2 to be immediately injected into the V^{5+} species, leaving back holes on the TiO_2 resulting in the effective separation of e^- and h^+ [37]. The V^{4+} species, created from V^{5+} by electron trapping, easily release and transfer the electron to oxygen molecule absorbed on the surface of TiO_2 to produce superoxide radicals $O_2^{\bullet-}$. The holes in the VB react with H_2O to produce hydroxyl radicals that are strong oxidizing agents required for the degradation of the dye [38]. Lanthanum ions act as the hole trapping sites to decrease the recombination process. The charge imbalance caused by titanium entering into the lattice of La_2O_3 during heat treatment reduces Ti^{4+} to Ti^{3+}, which act as hole traps [17]. However, both dopants

should be incorporated in an optimum concentration into TiO_2 because above this amount the same trapping sites act as the recombination centers.

Fig.8. Possible photocatalytic mechanism of the V-La co-doped TiO_2 under sun-like irradiation.

3.2.2. Relation between adsorption properties and photocatalytic activity

The correlation between photocatalytic performance and adsorption properties of all catalysts is shown in Fig. 9. The results show that all doped TiO_2 samples had a better adsorption capacity than the pure TiO_2. Adsorption capacity of powders increased with the increase of La and V ion doping. The factors leading to the enhanced adsorption capacity involve the change of the physical properties owing to doping, in our case: the larger specific surface area and pore volume are beneficial to achieve better adsorption of RB. From the results in Table 2, it can be seen that with very low content of V ions as a dopant, there is a significant increase in specific surface area and adsorption, probably due to its position on the catalyst surface.

Fig. 9 illustrates that the photocatalytic activity does not follow the changes of the adsorption ability. The adsorption is necessary precondition for the photocatalytic process, but it is not obligatory the large adsorption ability stimulates a faster degradation of the pollutant. It can be observed the increase of photoactivity with increasing adsorption, for La and also for V-La co-doped samples, until a certain amount of dopants. For sample with 4% La and co-doped TiO_2 with 2% La and 0.05% V ions, despite the best adsorption properties, there is a significant decrease in photoactivity. This indicates that some other effects influence the degradation efficiency. This low efficiency is mainly due to the fast recombination of charge carriers and this effect predominates.

Fig.9. Sorption and photocatalytic activity of the studied TiO_2 photocatalysts. Operating conditions: $[RB]_0 = 100$ mg L^{-1}, photocatalysts = 1 g L^{-1} and native pH.

3.2.3. Effect of the initial RB concentration and catalyst loading

Since the effect of pollutant concentration on the efficiency of water treatment is very important, it is necessary to investigate its dependence. The initial concentration of the dye is varied in the range from 50 to 140 mg L^{-1}, keeping constant the catalyst loading at 1.0 g L^{-1} and the results are presented in Fig. 10. It was found that percentage of dye removal decreases with the increase of initial dye concentration, which is often observed in the photocatalysis [35,39]. This can be explained by the fact that the generation of OH• radicals on the catalyst surface is reduced, since the active sites are occupied by dye ions. Also, increasing dye concentration leads to an increse of the amount of photons which are absorbed by the pollutant molecules and causes a decrease in the number of photons available for catalyst surface [40,41].

Fig.10. Effect of the initial RB concentration on the photocatalytic decolorization with 0.02V-2La/TiO_2 catalyst (1 g L^{-1}) over the concentration range of dye 50–140 mg L^{-1}.

Also, we examined the effect of catalyst loading on the photocatalytic degradation of 100 ml aqueous solution of RB dye (100 mg L^{-1}) was studied by varying the amount of 0.02V-2La/TiO_2 from 0.2 to 1 g L^{-1} and the results are presented in Fig. 11. The degradation was found to increase with the increasing concentration of catalyst to a certain point, where it reaches its maximum. That can be explained by increasing the number of active sites with increasing concentration of catalyst, but increase of the catalyst loading above an optimum value has no effect on the photodegradation

rate since all the light available is already utilized. It can be seen that plateau appears and only a slight decrease occurs. This is a very positive feature of the catalyst, because it means there is no aggregation of catalyst particles and the light scattering is not pronounced at higher catalyst's loading [41].

Fig.11. Effect of 0.02V-2La/TiO_2 loading on the efficiency of RB (100 mg L^{-1}) photodecolorization in the range from 0.2 to 1 g L^{-1}, for 40 minutes.

3.2.5. Sedimentation rate profile

After the degradation of pollutant, separation of photocatalyst is necessary. Sometimes, it is a serious problem, because the large specific surface area is required for efficient photocatalysis and therefore the catalyst particles are very fine, which complicates separation. It is very important to separate efficiently nanoparticles, because of their potential adverse effects on biological systems. To date, in the literature there is a little toxicological information about nanomaterials, and usually related to their effects by inhalation. Because of their huge surface area, particles may interact more efficiently with biological systems producing grave toxicity. Also, in the environment nanoparticles tend to form aggregates and thus provide ability for other organic materials, including pollutants, to become associated with the aggregates, which will create additional toxicological concerns [42].

In order to make the environmental application of TiO_2 photocatalysis more practical, immobilization of TiO_2 on the different substrates is performed. In the solar systems for water treatment, TiO_2 can be allowed to settle down during the night. The sedimentation rate of the 0.02V-2La/TiO_2 photocatalyst suspension was examined. After the stopping of stirring of the 0.3 g L^{-1} catalyst suspension, aliquots were taken at the appropriate time intervals. Sedimentation profile is shown in Fig. 12 and it was compared to the commercially available TiO_2 Evonik P25.

Fig.12. Comparison of the sedimentation rate between 0.02V-2La/TiO_2 catalyst and commercially available TiO_2 Evonik P25.

As shown in Fig. 12, 0.02V-2La/TiO_2 catalyst can be separated from an aqueous suspension in less than 4 h by sedimentation, while the aqueous suspension of Evonik P25 was still turbid even after 24 hours. Since the synthesized TiO_2 spontaneously precipitated, it was not necessary to add any coagulants or any electrolytes to the reaction mixtures. This is a great advantage over Evonik P25.

3.2.6. Photocatalytic activity of the recycled 0.02V-2La/TiO_2

Fig.13. Photodecolorization of RB by 0.02V-2La/TiO_2 catalyst in three successive catalytic cycles. Operating conditions: $[RB]_0$ = 50 mg L^{-1}, photocatalysts = 1 g L^{-1} and native pH.

After a photocatalytic treatment and separation of catalyst, one of the main requirements for the commercial applications of the catalyst is its reusability. In order to examine reusability of the 0.02V-2La/TiO_2 catalyst, after the process of decolorization, nanoparticles were collected, dried at 110 °C and reused in three successive photodegradation cycles. Each cycle lasted for 5 h.

Fig. 13 shows that the photodegradation degree of RB in five successive catalytic cycles was nearly the same. The results show that 0.02V-2La/TiO_2 catalyst is photochemically stable and there is no

need for additional procedures for the regeneration of the catalyst, such as thermal or treatment with H_2O_2 under UV irradiation [43], so it is acceptable for industrial application.

4. Conclusion

La doped and V-La co-doped TiO_2 photocatalysts were synthesized by the microwave-hydrothermal method. The La and V doping influenced morphological and textural characteristics of the synthesized photocatalysts, both dopants increase specific surface area and pore volume, as well as, reduce the size of aggregates, which are the critical parameters to enhance the photocatalytic activity. Vanadium doping plays a role in extending light absorption into the visible region. The La doped TiO_2 exhibits higher photoactivity than the pure TiO_2 and the presence of V ions in the co-doped samples additionally contributes to enhancement of photoactivity. The highest activity showed the catalyst with 2% La and 0.02% V, which are the optimal amounts of dopants, for the best balance between the increase in the adsorption and detrimental effect of fast recombination of charge carriers. The V-La co-doped catalyst showed better photocatalytic activity and sedimentation properties than Evonik P25. High efficiency of photocatalytic degradation under sun-like irradiation, the ability to achieve satisfactory separation by settling down and excellent photostability and reusability, make the V-La co-doped catalyst eco-friendly and cost saving for industrial application.

Acknowledgement

This work is supported by the Ministry for Science, Republic of Serbia (Project No. 172030).

References

[1] R. Andreozzi, V. Caprio, A. Insola, R. Marotta, Advanced oxidation processes (AOP) for water purification and recovery, Catal. Today 53 (1999) 51–59.
[2] S. Esplugas, J. Gimenez, S. Contreras, E. Pascual, M. Rodriguez, Comparison of different advanced oxidation processes for phenol degradation, Water Res. 36 (2002) 1034–1042.
[3] C. Pulgarin, J. Kiwi, V. Nadtochenko, Mechanism of photocatalytic bacterial inactivation on TiO_2 films involving cell-wall damage and lysis, Appl. Catal. B. Environ. 128 (2012) 179– 183.
[4] V. Augugliaro, V. Loddo, M. Pagliaro, G. Palmisano, L. Palmisano, Clean by light irradiation: Practical applications of supported TiO_2, The Royal Society of Chemistry, Cambridge, 2010.
[5] F. Mazille, T. Schoettl, C. Pulgarin, Synergistic effect of TiO2 and iron oxide supported on fluorocarbon films. Part 1: Effect of preparation parameters on photocatalytic degradation of organic pollutant at neutral pH, Appl. Catal. B. Environ. 89 (2009) 635–644.
[6] P. Sathishkumar, S. Anandan, P. Maruthamuthu, T. Swaminathan, M. Zhou, M. Ashokkumar, Synthesis of Fe^{3+} doped TiO_2 photocatalysts for the visible assisted degradation of an azo dye, Colloids Surf. A 375 (2011) 231–236.
[7] G. Colon, M. Maicu, M.C. Hidalgo, J.A. Navio, Cu-doped TiO_2 systems with improved photocatalytic activity, Appl. Catal. B. Environ. 67 (2006) 41–51.
[8] N. Couselo, F.S.G. Einschlag, R. J. Candal, M. Jobbágy, Tungsten-Doped TiO_2 vs Pure TiO_2 Photocatalysts: Effects on Photobleaching Kinetics and Mechanism, J. Phys. Chem. C 112 (2008) 1094–1100.
[9] S. Klosek, D. Raftery, Visible Light Driven V-Doped TiO_2 Photocatalyst and Its Photooxidation of Ethanol, J. Phys. Chem. B 105 (2001) 2815–2819.

[10] B. Liu, X. Wang, G. Cai, L. Wen, Y. Song, X. Zhao, Low temperature fabrication of V-doped TiO_2 nanoparticles, structure and photocatalytic studies, J. Hazard. Mater. 169 (2009) 1112–1118.

[11] D.B. Hamal, K.J. Klabunde, Valence State and Catalytic Role of Cobalt Ions in Cobalt TiO_2 Nanoparticle Photocatalysts for Acetaldehyde Degradation under Visible Light, J. Phys. Chem. C 115 (2011) 17359–17367.

[12] V. Stengl, S. Bakardjieva, Molybdenum-Doped Anatase and Its Extraordinary Photocatalytic Activity in the Degradation of Orange II in the UV and vis Regions, J. Phys. Chem. C 114 (2010) 19308–19317.

[13] Q.R. Deng, X.H. Xia, M.L. Guo, Y. Gao, G. Shao, Mn-doped TiO_2 nanopowders with remarkable visible light photocatalytic activity, Mater. Lett. 65 (2011) 2051–2054.

[14] J. Zhu, Z. Deng, F. Chen, J. Zhang , H. Chen, M. Anpo, J. Huang, L. Zhang, Hydrothermal doping method for preparation of Cr^{3+}-TiO_2 photocatalysts with concentration gradient distribution of Cr^{3+}, Appl. Catal. B. Environ. 62 (2006) 329–335.

[15] W. Choi, A. Termin, M. R. Hoffmann, The Role of Metal Ion Dopants in Quantum-Sized TiO_2: Correlation between Photoreactivity and Charge Carrier Recombination Dynamics, J. Phys. Chem. 98 (1994) 13669-13679.

[16] Y. Zhang, H. Zhang, Y. Xu, Y. Wang, Significant effect of lanthanide doping on the texture and properties of nanocrystalline mesoporous TiO_2, J. Solid State Chem. 177 (2004) 3490–3498.

[17] F.B. Li, X.Z. Li, M.F. Hou, Photocatalytic degradation of 2-mercaptobenzothiazole in aqueous La^{3+}–TiO_2 suspension for odor control, Appl. Catal. B. Environ. 48 (2004) 185–194.

[18] Q. Wang, S. Xu, F. Shen, Preparation and characterization of TiO_2 photocatalysts co-doped with iron (III) and lanthanum for the degradation of organic pollutants, Appl. Surf. Sci. 257 (2011) 7671–7677.

[19] W-G. Yang, F-R. Wan, Q-W. Chen, J-J. Li, D-S. Xu, Controlling synthesis of well-crystallized mesoporous TiO_2 microspheres with ultrahigh surface area for high-performance dye-sensitized solar cells, J. Mater.Chem. 20 (2010) 2870–2876.

[20] J. Zhang, X. Xiao, J. Nan, Hydrothermal-hydrolysis synthesis and photocatalytic properties of nano-TiO_2 with an adjustable crystalline structure, J. Hazard. Mater. 176 (2010) 617–622.

[21] M. Addamo, M. Bellardita, D. Carriazo, A. Paola, S. Milioto, L. Palmisano, V. Rives, Inorganic gels as precursors of TiO2 photocatalysts prepared by low temperature microwave or thermal treatment, Appl. Catal. B. Environ. 84 (2008) 742–748.

[22] G. Wilson, G. W. Frost, S. Montgomery, Efficient microwave hydrothermal preparation of nanocrystalline anatase TiO_2 colloids, J. Mater. Chem. 12 (2002) 1787–1791.

[23] J. Rodríguez-Carvajal: FullProf Suite: Crystallographic tools for Rietveld, profile matching & integrated intensity refinements of X-ray and/or neutron data. http://www.ill.eu/sites/fullprof/

[24] F. Rouquerol, J. Rouquerol, K. Sing, Adsorption by Powders and Porous Solids, Principles, Methodology and Applications, Academic Press, London, 1999.

[25] S.J. Gregg, K.S.W. Sing, Adsorption, Surface Area and Porosity, Academic Press, London, 1982.

[26] Press, NY, 1975. M.M. Dubinin, Progress in Surface and Membrane Science, vol. 9, Academic.

[27] E.P. Barrett, L.G. Joyner, P.P. Halenda, The Determination of Pore Volume and Area Distributions in Porous Substances. I Computations from Nitrogen Isotherms, J. Am. Chem. Soc. 73 (1951) 373–380.

[28] A. Xu, Y. Gao, H. Liu, The Preparation, Characterization, and their Photocatalytic Activities of Rare-Earth-Doped TiO_2 Nanoparticles, J. Catal. 207 (2002) 151–157.

[29] K. Bhattacharyya, S. Varma, A. K. Tripathi, S. R. Bharadwaj, A. K. Tyagi, Effect of Vanadia Doping and Its Oxidation State on the Photocatalytic Activity of TiO_2 for Gas-Phase Oxidation of Ethene, J. Phys. Chem. C 112 (2008) 19102–19112.
[30] S. Chang, W. Liu, Surface doping is more beneficial than bulk doping to the photocatalytic activity of vanadium-doped TiO_2, Appl. Catal. B. Environ. 101 (2011) 333–342.
[31] I.K. Konstantinou, T.A. Albanis, TiO_2-assisted photocatalytic degradation of azo dyes in aqueous solution: kinetic and mechanistic investigations: A review, Appl. Catal. B. Environ. 49 (2004) 1–14.
[32] D. Bahnemann, M. Hilgendorff, R. Memming, Charge Carrier Dynamics at TiO_2 Particles: Reactivity of Free and Trapped Holes, J. Phys. Chem. B 101 (1997) 4265-4275.
[33] Z. Zhang, C. Wang, R. Zakaria, J.Y. Ying, Role of Particle Size in Nanocrystalline TiO_2-Based Photocatalysts, J. Phys. Chem. B 102 (1998) 10871-10878.
[34] J. Haber, T. Machej, E.M. Senvicka, I.E. Wachs, Mechanism of surface spreading in vanadia-titania system, Catal. Lett. 32 (1995) 101-114.
[35] C.S. Turchi, D.F. Ollis, Photocatalytic degradation of organic water contaminants: Mechanisms involving hydroxyl radical attack, J. Catal. 122 (1990) 178–185.
[36] S. Liu, T. Xie, Z. Chan, J. Wu, Highly active V–TiO_2 for photocatalytic degradation of methyl orange, Appl. Surf. Sci. 255 (2009) 8587–8592.
[37] R. Dholam, N. Patel, A. Miotello, Efficient H_2 production by water-splitting using indiumetin-oxide/V-doped TiO_2 multilayer thin film photocatalyst, Int. J. Hydrogen Energy 36 (2011) 6519–6528.
[38] Y. Wang, Y.R. Su, L. Qiao, L.X. Liu, Q. Su, C.Q. Zhu, X.Q. Liu, Synthesis of one-dimensional TiO_2/V_2O_5 branched heterostructures and their visible light photocatalytic activity towards Rhodamine B, Nanotechnology 22 (2011) 225702–225709.
[39] J. Cunningham, G. Al-Sayyed, P. Sedlak, J. Caffrey, Aerobic and anaerobic TiO_2-photocatalysed purifications of waters containing organic pollutants, Catal. Today 53 (1999**)** 145-158.
[40] F. Kiriakidou, D.I. Kondarides, X.E. Verykios, The effect of operational parameters and TiO_2-doping on the photocatalytic degradation of azo-dyes, Catal. Today 54 (1999) 119–130.
[41] N. Banić, B. Abramović, J. Krstic, D. Šojic, D. Lončarević, Z. Cherkezova-Zheleva, V. Guzsvany, Photodegradation of thiacloprid using Fe/TiO_2 as a heterogeneous photo-Fenton catalyst, Appl. Catal. B. Environ. 107 (2011) 363– 371.
[42] A.D. Servin, H. Castillo-Michel, J.A. Hernandez-Viezcas, B. Corral, J.R. Peralta-Videa, J.L. Gardea-Torresdey, Synchrotron Micro-XRF and Micro-XANES Confirmation of the Uptake and Translocation of TiO2 Nanoparticles in cucumber (Cucumis sativus) Plants, Environ. Sci. Technol. 46 (2012) 7637−7643.
[43] F. Han, V.S.R. Kambala, M. Srinivasan, D. Rajarathnam, R. Naidu, Tailored titanium dioxide photocatalysts for the degradation of organic dyes in wastewater treatment: A review, Appl. Catal. A-Gen. 359 (2009) 25-40.

Sample	Unit cell parameters		Microstructure parameters		Rietveld refinement residuals				
	a(Å)	c(Å)	Average size (Å)	Average strain ($\times 10^{-3}$)	R_p	R_{wp}	R_{exp}	χ^2	R_B
TiO_2	3.7860(2)	9.5032(7)	175	24	7.4	10.2	8.1	1.59	2.29
2La/TiO_2	3.7878(4)	9.4982(9)	84	37	8.0	10.7	9.0	1.41	2.21
4La/TiO_2	3.7883(5)	9.4902(10)	79	30	9.3	11.7	10.1	1.34	2.59
0.01V-2La/TiO_2	3.7872(4)	9.4913(9)	94	35	8.3	10.5	9.1	1.30	1.44
0.02V-2La/TiO2	3.7868(4)	9.4938(9)	86	30	7.8	10.2	9.2	1.22	1.32
0.05V-2La/TiO2	3.7871(4)	9.4883(9)	82	29	8.3	10.7	9.2	1.36	1.57

Sample code	Content (wt.%)			S_{BET} (m^2 g^{-1})	V_{tot} (cm^3 g^{-1})	V_{mic} (cm^3 g^{-1})	V_{meso} (cm^3 g^{-1})	Pore diametar (nm)
	La	Ti	V					
TiO_2	-	58.83	-	65.7	0.236	0.018	0.206	10.2
$0.2La/TiO_2$	0.22	57.12	-	88.4	0.267	0.026	0.239	8.7
$2La/TiO_2$	1.84	55.51	-	120	0.339	0.036	0.297	7.5
$4La/TiO_2$	4.48	54.02	-	123	0.366	0.037	0.322	7.7
$0.01V\text{-}2La/TiO_2$	1.99	54.39	0.01	116	0.322	0.035	0.284	7.5
$0.02V\text{-}2La/TiO_2$	1.98	53.59	0.02	125	0.348	0.036	0.284	6.8
$0.05V\text{-}2La/TiO_2$	2.19	53.56	0.05	132	0.372	0.039	0.327	7.7

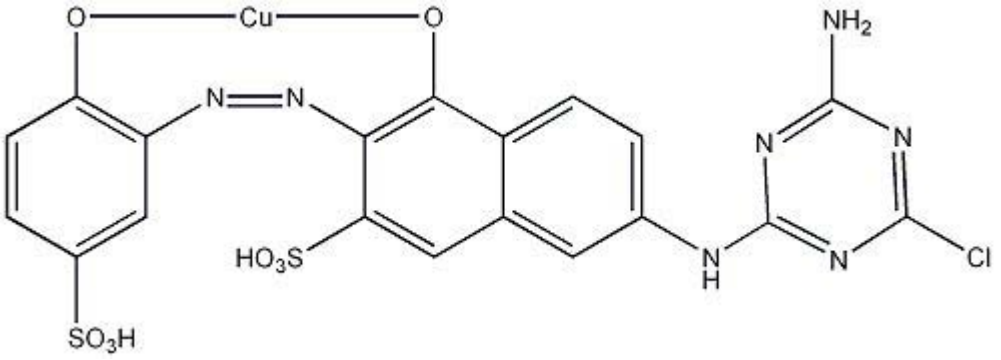
O
Cu
O
N=N
NH2
N
N
HO3S
N
H
N
Cl
SO3H

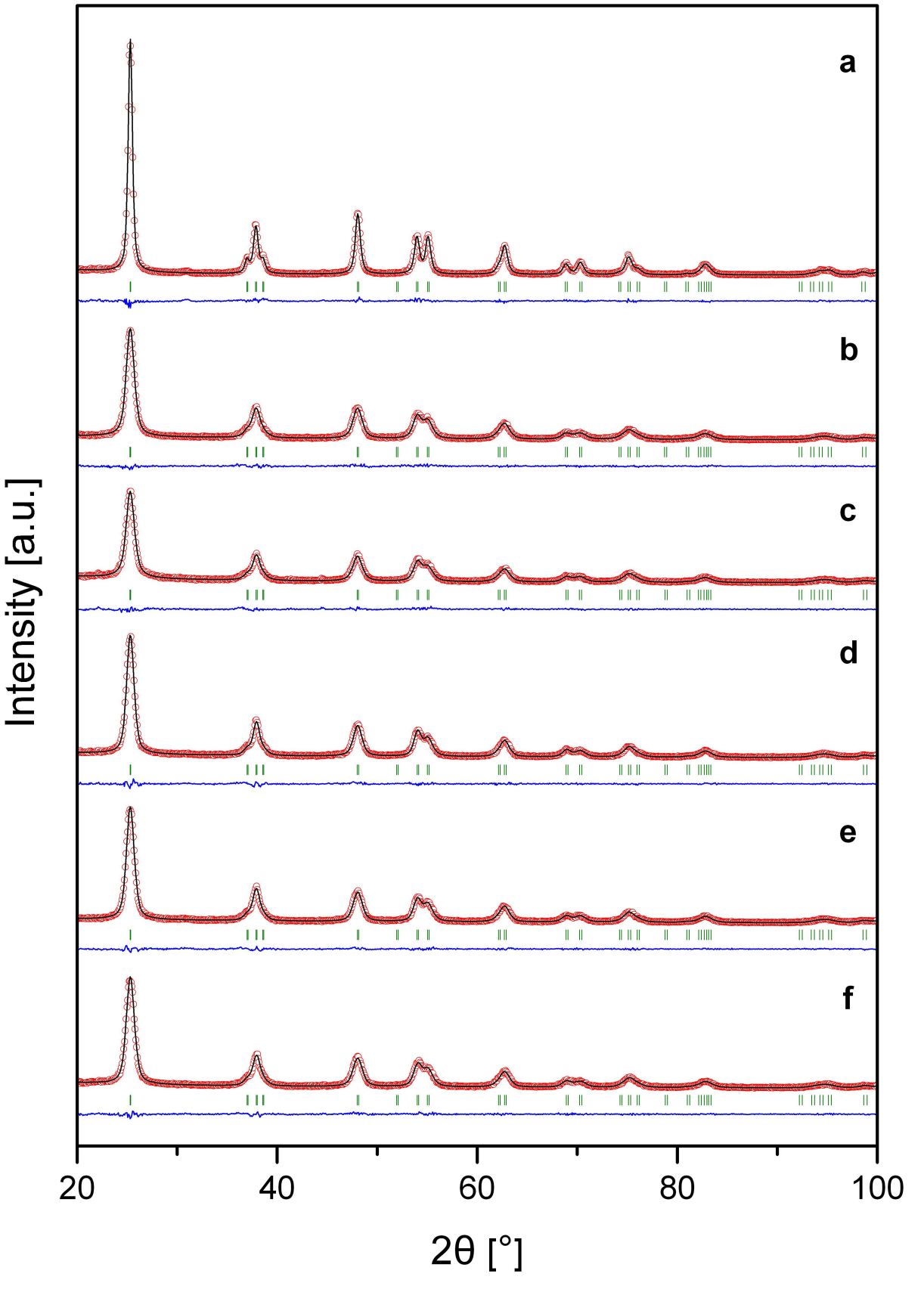
a
b
c
d
e
f
Intensity [a.u.]
20
40
60
80
100
2θ [°]

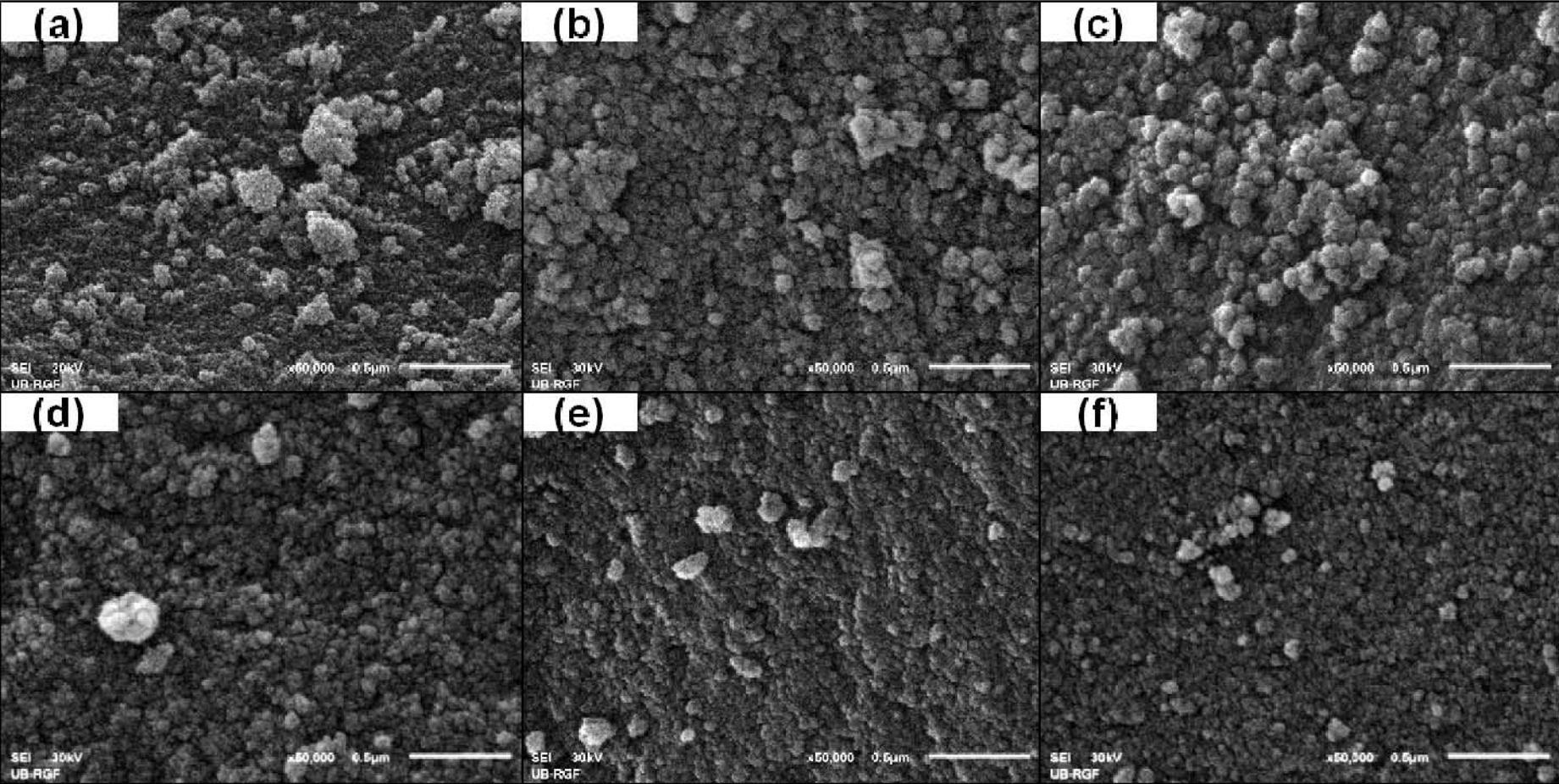
(a)
(b)
(c)
(d)
(e)
(f)

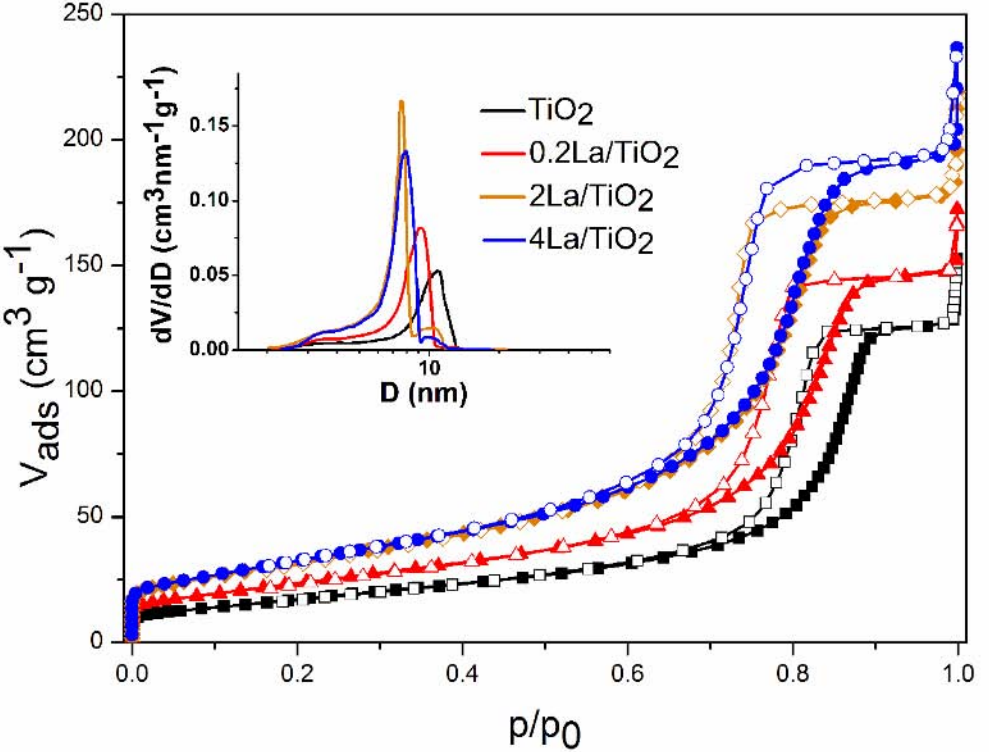
250
200
150
100
50
0
0.0
0.2
0.4
0.6
0.8
1.0
V_{ads} (cm^3 g^{-1})
p/p_0
dV/dD ($cm^3nm^{-1}g^{-1}$)
0.15
0.10
0.05
0.00
10
D (nm)
TiO_2
0.2La/TiO_2
2La/TiO_2
4La/TiO_2

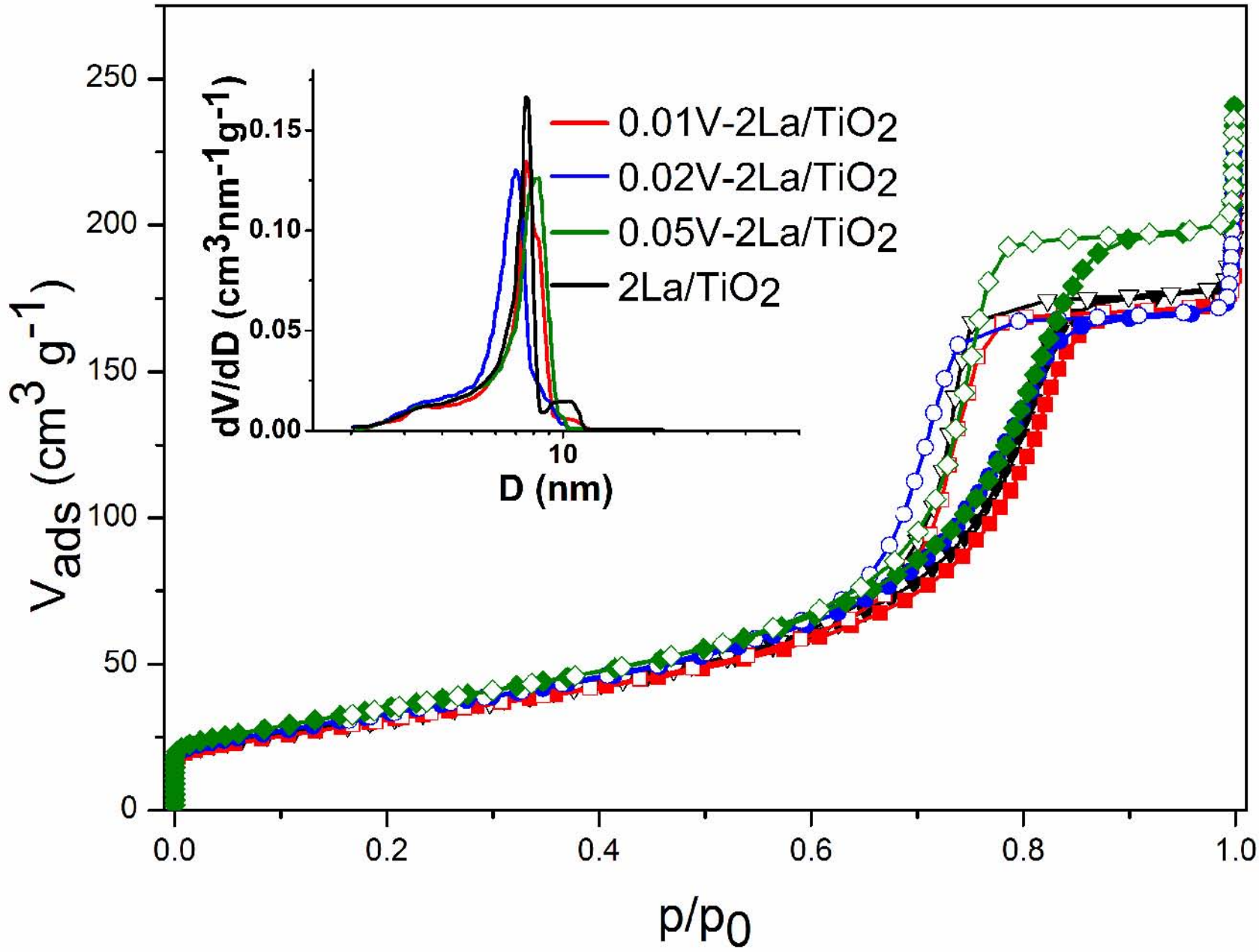
250
200
150
100
50
0
0.0
0.2
0.4
0.6
0.8
1.0
V_{ads} (cm^3 g^{-1})
p/p_0
0.01V-2La/TiO_2
0.02V-2La/TiO_2
0.05V-2La/TiO_2
2La/TiO_2
dV/dD ($cm^3nm^{-1}g^{-1}$)
0.15
0.10
0.05
0.00
10
D (nm)

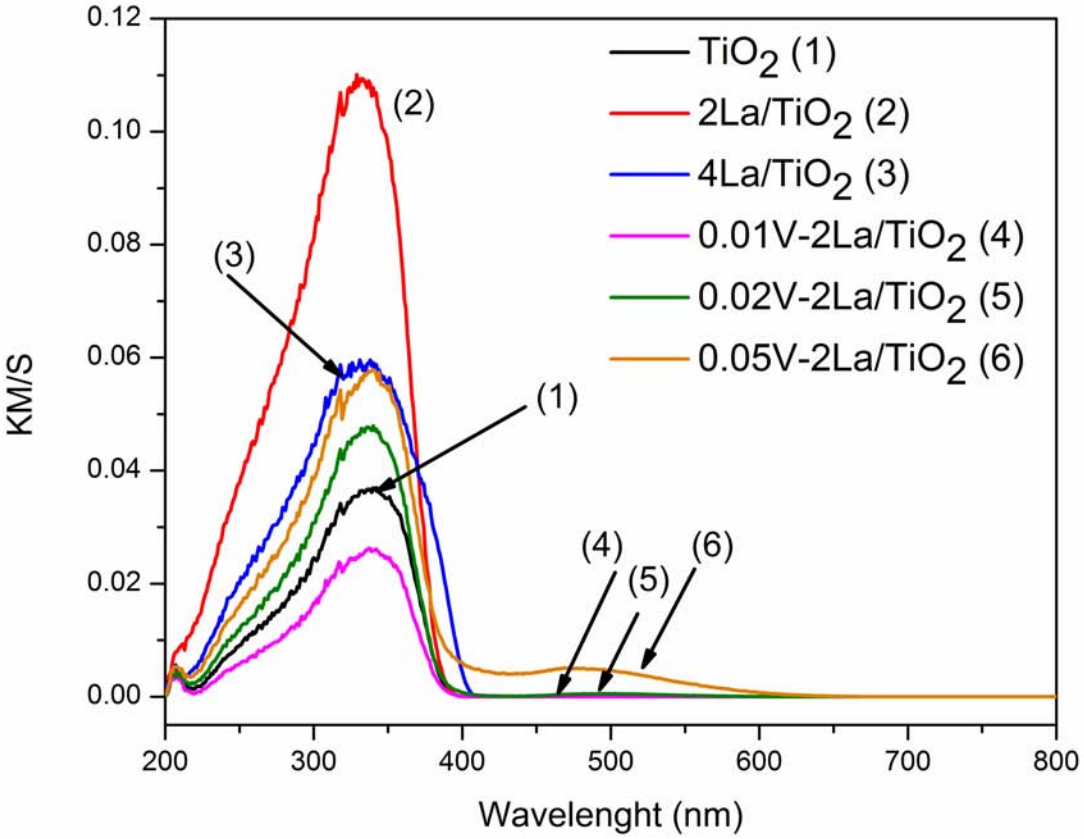
0.12
0.10
0.08
0.06
0.04
0.02
0.00
KM/S
200
300
400
500
600
700
800
Wavelenght (nm)
TiO2 (1)
2La/TiO2 (2)
4La/TiO2 (3)
0.01V-2La/TiO2 (4)
0.02V-2La/TiO2 (5)
0.05V-2La/TiO2 (6)
(1)
(2)
(3)
(4)
(5)
(6)

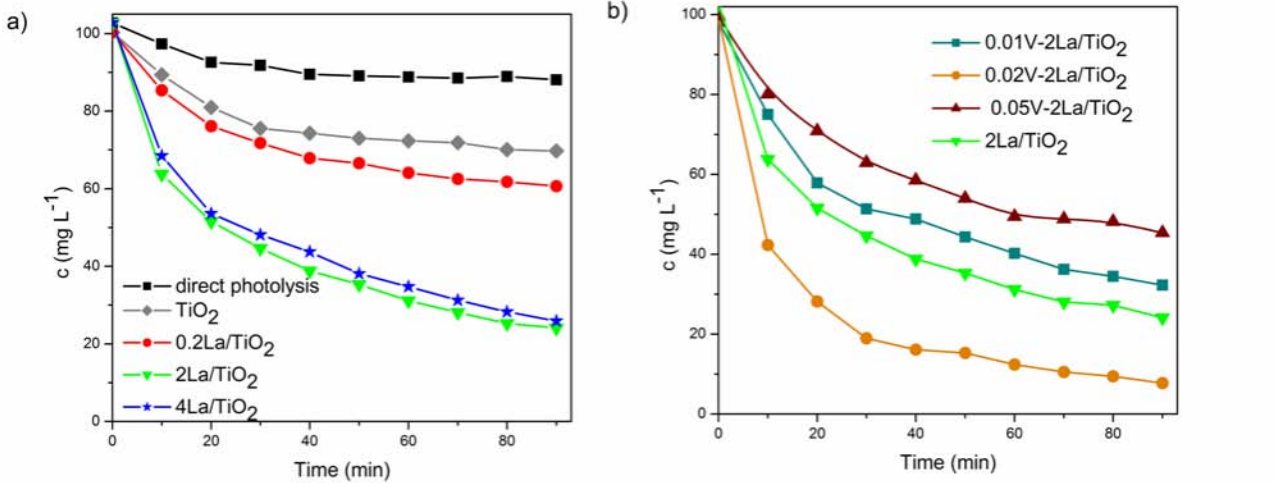
a)
c (mg L-1)
Time (min)
direct photolysis
TiO2
0.2La/TiO2
2La/TiO2
4La/TiO2
b)
c (mg L-1)
Time (min)
0.01V-2La/TiO2
0.02V-2La/TiO2
0.05V-2La/TiO2
2La/TiO2

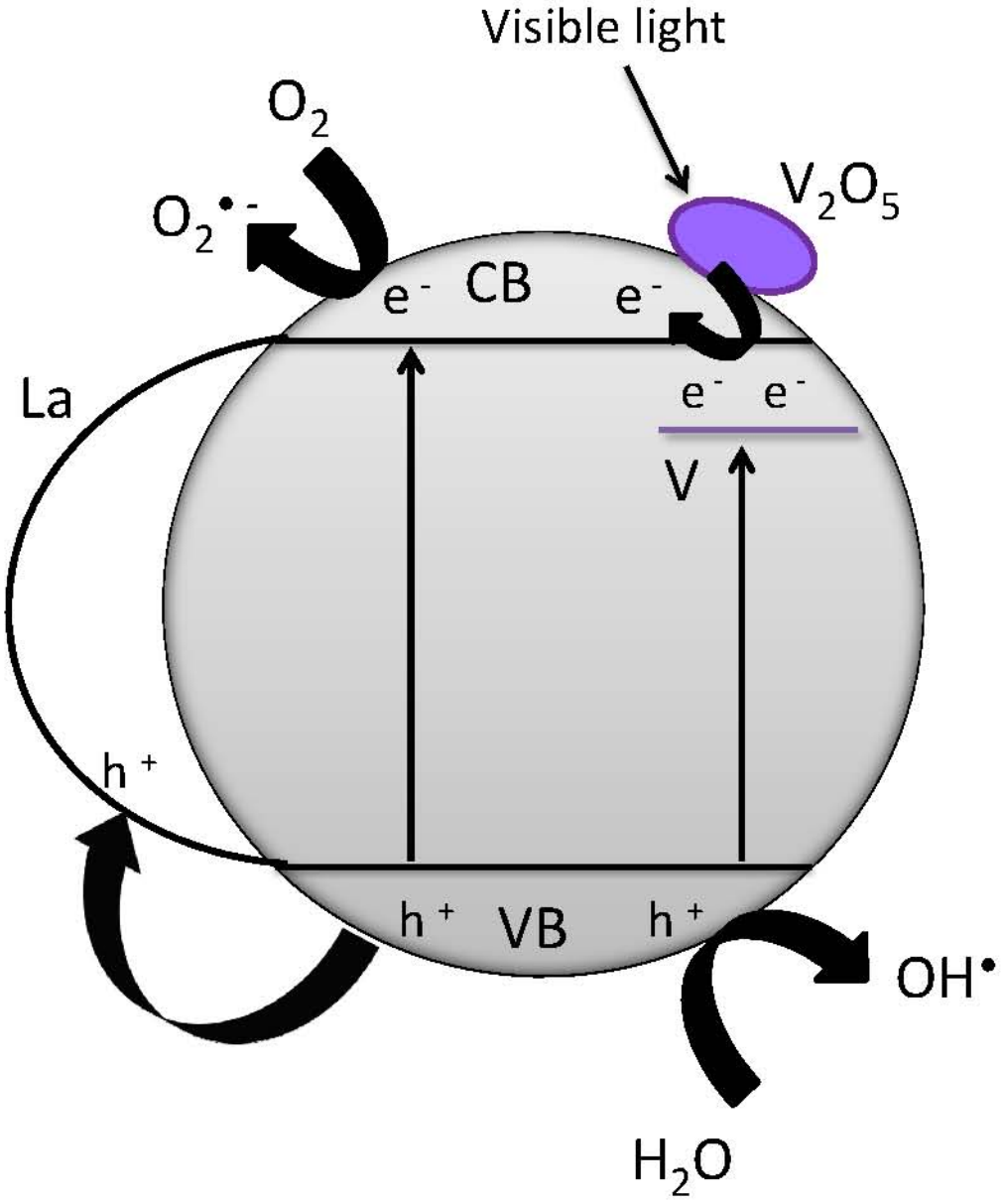
Visible light
O_2
$O_2^{\bullet -}$
V_2O_5
e^- CB
e^-
e^- e^-
V
La
h^+
h^+ VB h^+
$OH^\bullet$
H_2O

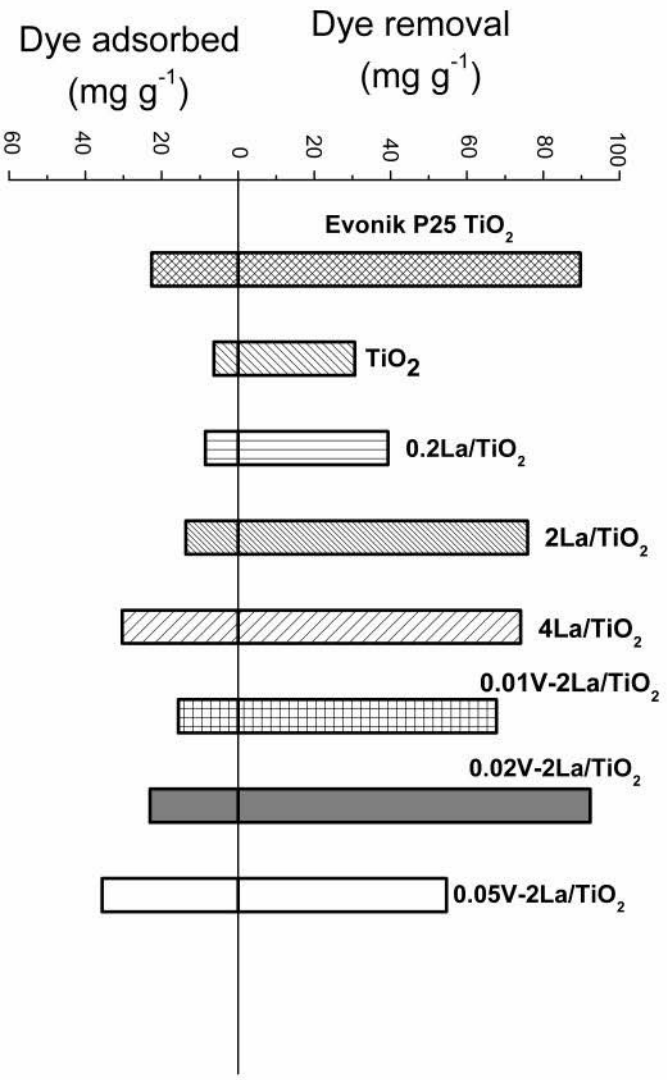
Dye adsorbed
(mg g-1)
Dye removal
(mg g-1)
60
40
20
0
20
40
60
80
100
Evonik P25 TiO2
TiO2
0.2La/TiO2
2La/TiO2
4La/TiO2
0.01V-2La/TiO2
0.02V-2La/TiO2
0.05V-2La/TiO2

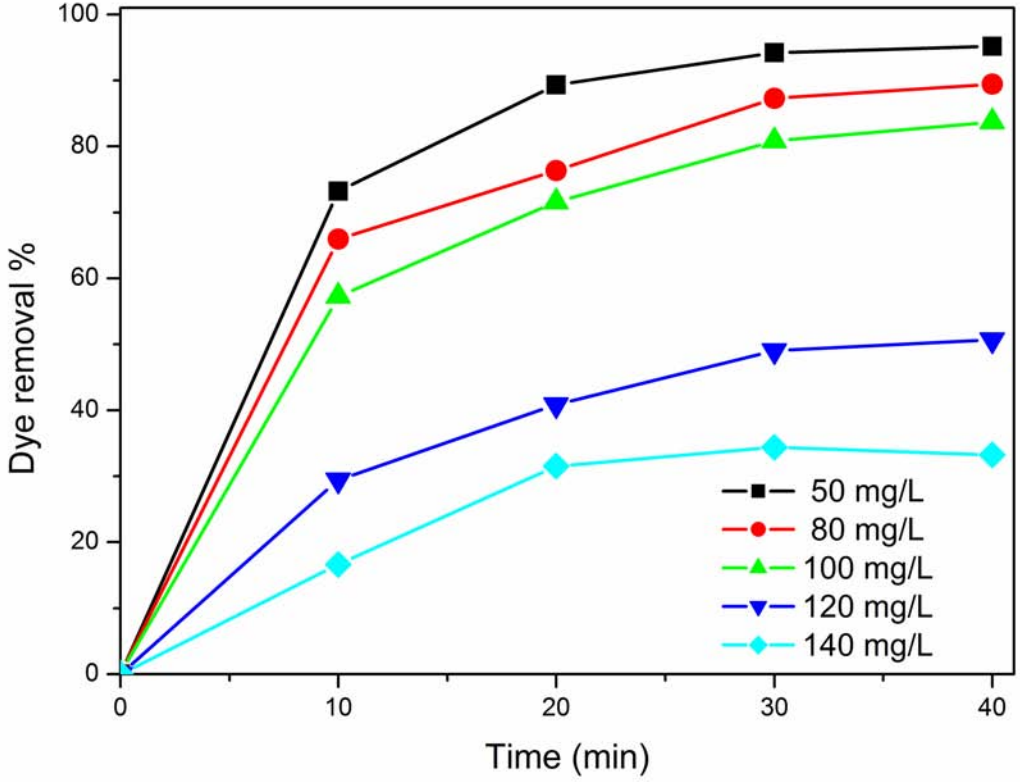
Dye removal %
Time (min)
0
20
40
60
80
100
0
10
20
30
40
50 mg/L
80 mg/L
100 mg/L
120 mg/L
140 mg/L

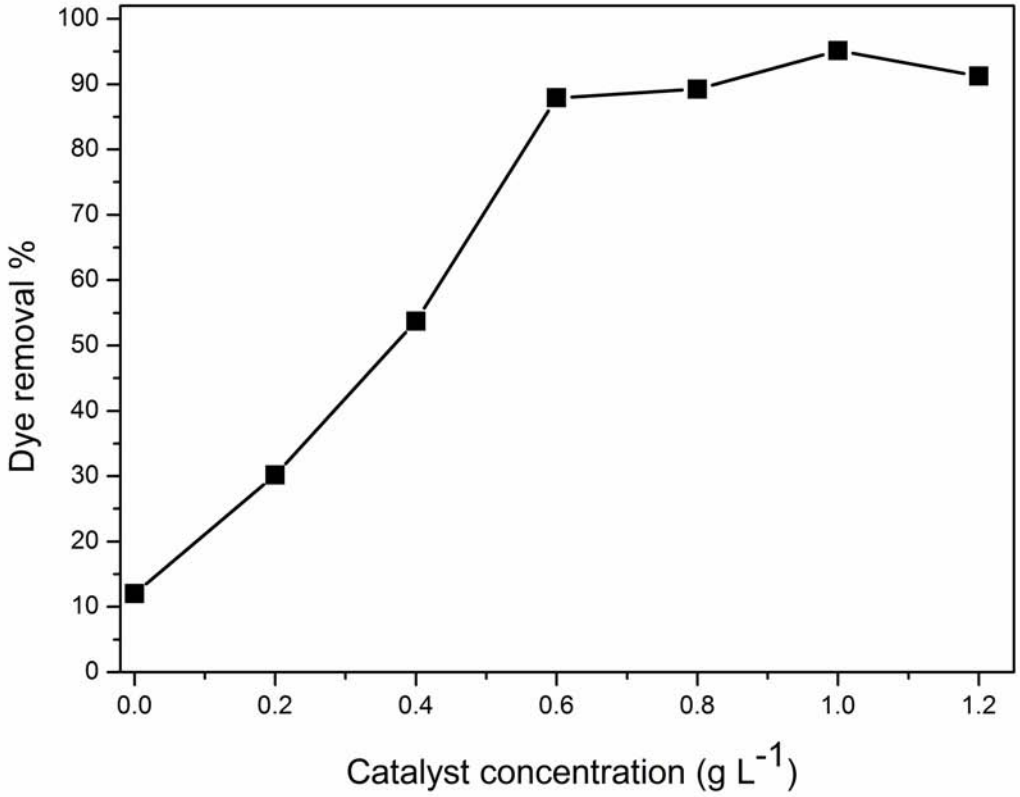
Dye removal %
100
90
80
70
60
50
40
30
20
10
0
0.0
0.2
0.4
0.6
0.8
1.0
1.2
Catalyst concentration (g L-1)

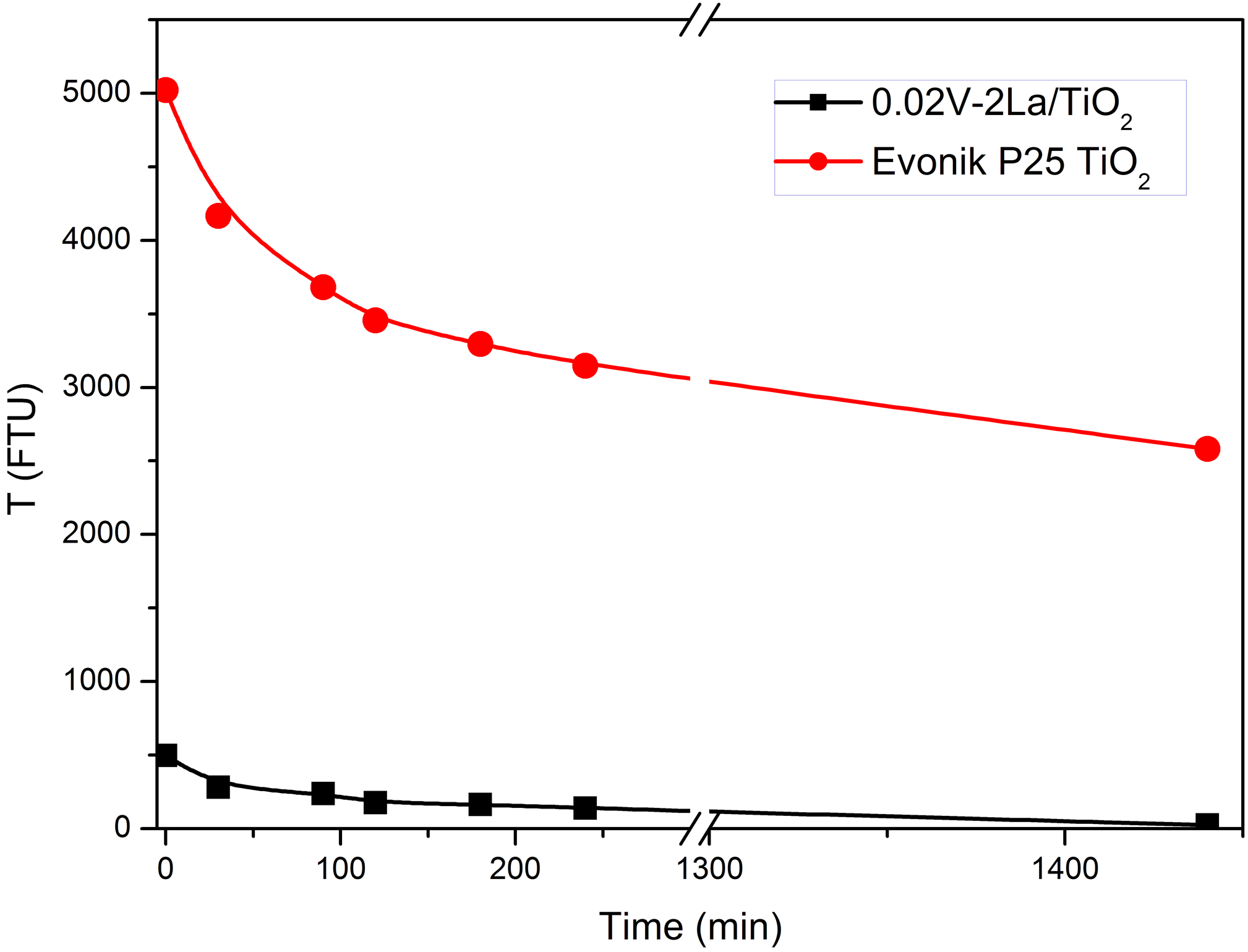
5000
4000
3000
2000
1000
0
T (FTU)
0
100
200
1300
1400
Time (min)
0.02V-2La/TiO2
Evonik P25 TiO2

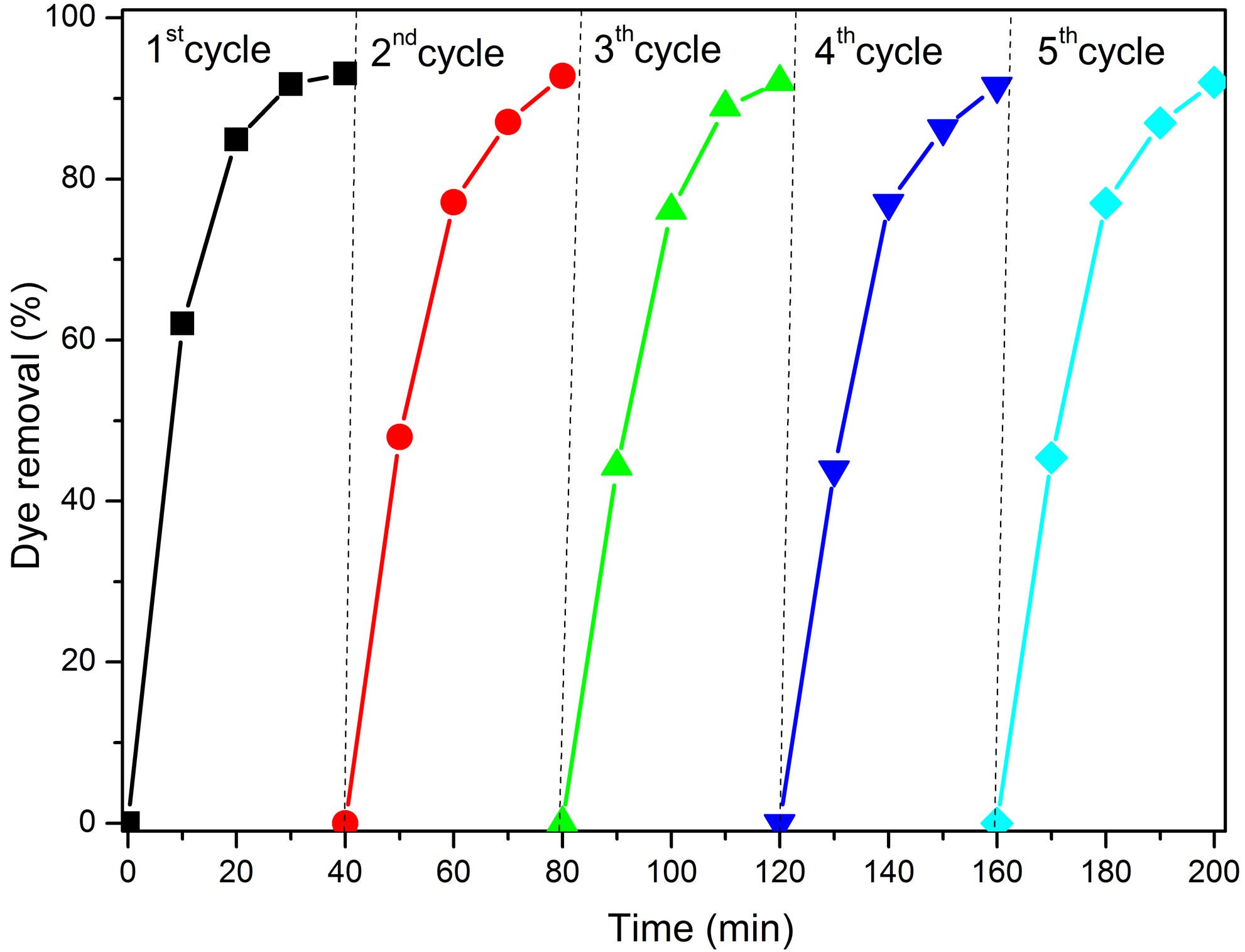
1st cycle
2nd cycle
3th cycle
4th cycle
5th cycle
Dye removal (%)
Time (min)
0
20
40
60
80
100
120
140
160
180
200